The journal version of this paper can be accessed in Nature Electronics
https://doi.org/10.1038/s41928-022-00798-8

How to Report and Benchmark Emerging Field-Effect Transistors

Zhihui Cheng[1,2,†], Chin-Sheng Pang[2], Peiqi Wang[3], Son T. Le[1,4], Yanqing Wu[5], Davood Shahrjerdi[6,7], Iuliana Radu[8], Max C. Lemme[9,10], Lian-Mao Peng[11], Xiangfeng Duan[3], Zhihong Chen[2], Joerg Appenzeller[2], Steven J. Koester[12], Eric Pop[13], Aaron D. Franklin[14,15,†], Curt A. Richter[1,†]

The use of organic, oxide and low-dimensional materials in field-effect transistors has now been studied for decades. However, properly reporting and comparing device performance remains challenging due to the interdependency of multiple device parameters. The interdisciplinarity of this research community has also led to a lack of consistent reporting and benchmarking guidelines. Here we propose guidelines for reporting and benchmarking key field-effect transistor parameters and performance metrics. We provide an example of this reporting and benchmarking process by using a two-dimensional semiconductor field-effect transistor. Our guidelines should help promote an improved approach for assessing device performance in emerging field-effect transistors, helping the field to progress in a more consistent and meaningful way.

Research into field-effect transistors (FETs) based on emerging nanomaterials, including carbon nanotubes[1,2], graphene[3], phosphorene[4], silicene[5], tellurene[6], transition metal dichalcogenides[7–9], organic semiconductors[10,11] and ultrathin metal oxides[12], is thriving. Such studies allow the fundamental properties of the materials to be explored, and may lead to the development of various commercial applications; however, effectively and uniformly assessing the performance of emergent FETs is difficult due to the dependence of performance metrics on unique aspects of the device structure (Fig. 1a)[13].

Structural parameters that influence device performance include channel (L_{ch}) and contact lengths (L_c), gate insulator thickness (t_{ins}) and permittivity (ϵ_{ins}), contact metal types, the thickness of channel material (t_{ch}), and gating scheme (e.g., top, bottom, gate-all-around, multi-channel). Performance metrics include on-current (I_{on}), off-current (I_{off}), I_{on}/I_{off} ratio, contact resistance (R_c), transconductance (g_m), subthreshold swing (SS), channel mobilities, and drain-induced barrier lowering (DIBL). While different studies reported in the literature often include some of these benchmarking figures, they struggle to capture the myriad variables, making comparisons inaccurate or even biased at times. In addition, the emerging device community consists of researchers from disparate disciplines — including electrical engineering, chemistry, materials science, and physics — which also makes consistent reporting and benchmarking challenging. In this Perspective, we examine the challenges involved in assessing the operation and performance of FETs based on emerging materials, and provide guidelines on how to report and benchmark the devices.

A full list of affiliations appears at the end of the paper.

Field-effect transistor structure and key parameters

In a FET, the structural parameters determine the electric fields and the eventual device performance (Fig. 1a). Subthreshold, transfer, and output characteristics in Figs. 1b-d are the most common *I-V* (current-voltage) curves to capture the device performance. Plotting the log of the drain current (I_D) as a function of gate-source voltage (V_{GS}) highlights the subthreshold (i.e., off-state) device behaviour. In contrast, transfer characteristics plot I_D vs. V_{GS} on a linear scale and emphasize the device behaviour after V_{GS} exceeds the threshold voltage (V_T), where the device is in the on-state. Ideally, the gate leakage current (I_G) vs. V_{GS} should be plotted on the subthreshold plot as well.

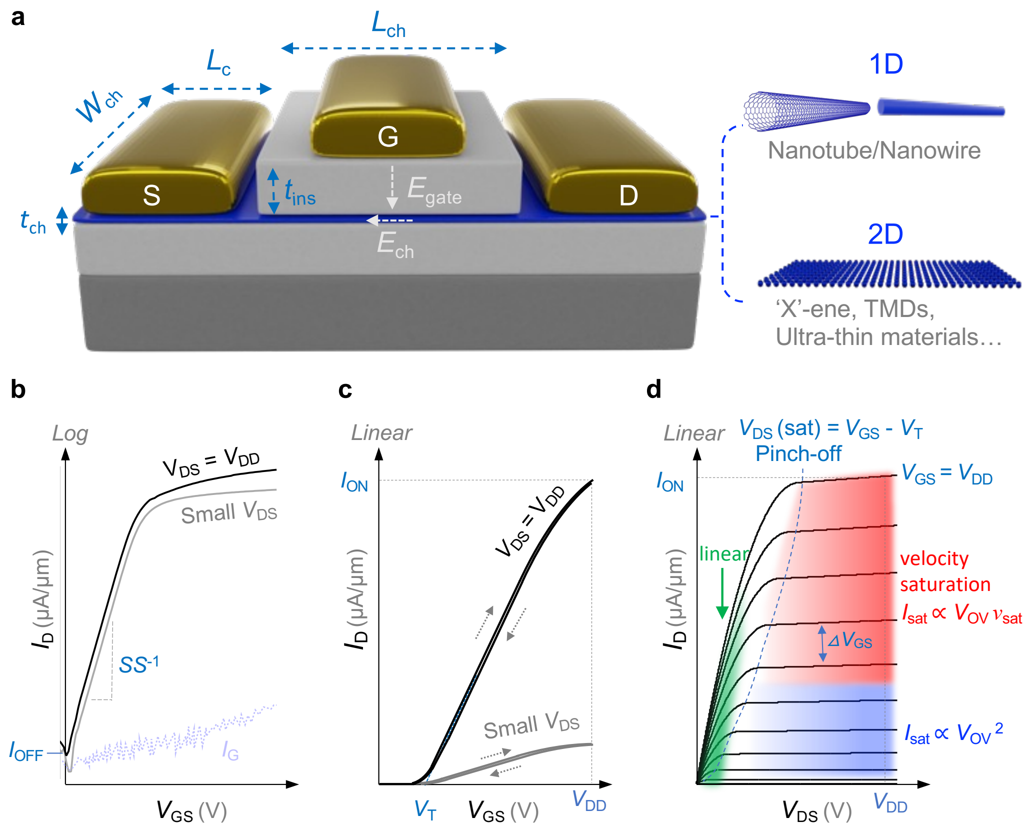

Fig. 1 | Basic device structure and electrical characteristics. **a**, Diagram of a typical nanomaterial-based n-type FET highlighting the structure parameters and electric fields. **b**, Subthreshold and **c**, transfer (I_D-V_{GS}) curves of an *n*-type FET under different V_{DS} voltages. Representative curves are shown for single-sweep in (**b**), but forward- and backward-sweeps of V_{GS} should be collected to determine hysteresis, as shown in (**c**). The gate leakage current is also shown in (**b**). **d**, Output (I_D-V_{DS}) curves of the device with three main operation regimes labelled.[14] V_{GS} is swept from low to high in steps of ΔV_{GS}. v_{sat} is the saturation velocity of carriers in the channel material. I_{sat} scales as V_{OV}^2 in the classical pinch-off regime, but only linearly with V_{OV} when the velocity saturates. Self-heating could render this increase even sub-linear.[14,15] Note, V_{DD} is the supply voltage for the transistor (i.e., the target maximum voltage of operation for both V_{DS} and V_{GS}).

The I_D-V_{GS} sweeps in Fig. 1b-c should be conducted at both "small" and "high" drain-source voltage (V_{DS}) values to characterize the device operation in both linear and saturation regimes. We note

that the "small" V_{DS} value should be sufficiently small to ensure linear regime operation, but greater than ~$2k_BT$ (where k_B is the Boltzmann constant and T is the absolute temperature, i.e., ~50 mV at room temperature) to ensure that the subthreshold behaviour, and here in particular DIBL ($\partial V_T/\partial V_{DS}$), is not misinterpreted due to thermal injection of carriers from the drain. These curves enable easy extraction of DIBL to demonstrate how V_{DS} impacts V_T. The transfer characteristics should be acquired with forward and backward sweeps, checking for the presence of any hysteresis due to charge trapping[16]. When comparing hysteresis from different devices, the precise measurement conditions such as sweep rates, hold times, and maximum bias voltages should be listed as these parameters influence hysteresis. If hysteresis exists, it should be accounted for in the analysis of V_T uncertainty and other device parameters that depend on V_T.

In the output characteristics (Fig. 1d), three main operation regimes are highlighted. The linear regime is characterized by the linear increase of I_D with both V_{DS} and V_{GS}. After V_{DS} surpasses the overdrive voltage ($V_{OV} = V_{GS} - V_T$, for *n*-channel FETs), I_D starts to saturate to I_{sat}, which could (based on the classical FET model[17]) increase quadratically with V_{OV} in the pinch-off regime and linearly with V_{OV} in the velocity saturation regime[14]. Note, the linear regime may present as nonlinear (often exponential) in the event of poor carrier injection at the contacts, such as from large Schottky barriers.

Multiple performance parameters can be extracted from the *I-V* curves in Fig. 1b-d. The most important performance metrics are the currents, which must be reported normalized by the channel width, W_{ch} (e.g., units of µA/µm). For 1D or quasi-1D devices, it is common to first report the current per CNT/nanowire/nanosheet stack. Then the current can be normalized to µA/µm by considering the expected channel density and pitch of the channel material (e.g., 10 µA/CNT with 50 CNTs/µm, giving 500 µA/µm) since the aerial footprint of the device is a critical aspect of performance. When extracting I_{on} and I_{off} from these *I-V* curves, in a simplified scenario, I_{off} is the I_D measured at $V_{GS} = 0$ and $V_{DS} = V_{DD}$, whereas I_{on} is the I_D measured at $V_{GS} = V_{DS} = V_{DD}$. Here, V_{DD} is the voltage that would be supplied to operate the transistors. (For mainstream silicon technology, V_{DD} has dropped to 1 V near 2010 and to 0.7 V in recent years[18].) For modern technologies, the exact value of V_{DD} depends on the application. For example, if the emergent transistor is used as an access transistor in a dynamic random-access memory (DRAM), then its V_{DD} will be a small value to ensure linear regime operation in the on-state. Reported emergent devices often do not have threshold voltages tuned such that $V_{GS} = 0$ is a sensible off-state; additionally, there is often not a well-defined V_{DD} value due to the wide variety of device structural parameters. We hence suggest extracting the maximum and minimum I_D (I_{max} and I_{min}) from

a typical subthreshold curve and reporting the I_{max}/I_{min} ratios when V_{DS} is biased in both linear and saturation regimes. A more detailed description on reporting and benchmarking I_{max}/I_{min} is in Note S1.

When reporting the I_{sat} of a device, it is necessary to note the carrier density n, at which the I_{sat} is extracted. Ideally, the Hall effect is used to measure the carrier density for the channel material, but for most researchers in the FET community, more accessible approaches are needed that do not require specially designed test structures. In the linear regime, the average carrier density can be estimated as $n \approx C_{ins} (V_{OV} - V_{DS}/2)/q$, where C_{ins} is the gate insulator capacitance and q is the elementary charge; however, in the saturation regime, the depletion region in the channel complicates the estimation. The carrier density *near the source side* is the same for both the linear and saturation regimes. For convenience and simplicity, we recommend clearly labelling the carrier density near the source as n_S ($= C_{ins} V_{OV}/q$) and using this value for both operation regimes. To determine V_{OV}, V_T is usually estimated using extrapolation in the linear portion of the transfer curve, as listed in Table 1. Other methods, such as constant current[19], Y-function methods[20,21] and four-probe measurements[22], can be used to cross-check the linear extraction of V_T and reduce the variation when estimating n_S. More discussion regarding V_T extraction is given in Note S2.

In addition to I_D, R_c is also essential to represent device performance. The transfer length method (TLM) is the most commonly used approach for extracting R_c, along with the sheet resistance, R_{sh}, of the channel (in units of Ω/square)[23]. The TLM approach requires a series of FETs with different channel lengths and consistent contact and gating configurations. It entails plotting the total resistance of each device versus L_{ch} at a given n_S, allowing R_c to be extracted as the extrapolated y-axis intercept from a linear fit to the data points. Typically, the V_{DS} for calculating the total resistance is the "small" V_{DS} used in Fig. 1b to ensure linear regime operation. The channel lengths in the TLM should range from "short" (where the total resistance is dominated by R_c) to "long" (dominated by channel resistance, $R_{ch} = R_{tot} - 2R_c$ or $R_{sh}L_{ch}$) where the actual "short" and "long" channel lengths will depend on the relationship between the channel resistance and the contact resistance. A more detailed discussion on extracting R_c and other considerations using TLM data is in Note S3.

Another frequently reported parameter is the carrier mobility of the channel material. Among various forms of mobility, the field-effect mobility $\mu_{FE} = L_{ch} g_m/(W_{ch} C_{ins} V_{DS})$ is often used. However, μ_{FE} can be underestimated[21,24] or overestimated[22,25,26] relative to the drift mobility of the channel material depending on the details of V_{DS}, V_{GS}, R_c, L_{ch}, and gate capacitance. In particular, gated contact effects can significantly affect mobility extraction. Although different approaches[21,23] have been proposed to make μ_{FE} less dependent on various factors, such as R_c and L_{ch}, none of them is sufficiently general

enough to be widely adopted. Conductivity mobility (μ_{con}) has the advantage of strictly reflecting the channel material properties and the quality of the channel-dielectric interface[23,27]. In a FET, μ_{con}[23] can be estimated from the sheet resistance of the semiconductor channel and the carrier density n_S (see Table 1); thus, it does not involve the contact resistance or the device structure. High mobility is often a goal for research FETs; when such reports are made, it is critical to clearly state how the values are determined, and ideally multiple approaches (such as μ_{FE} and four-probe measurements[22]) are taken to cross-validate the claims. It is worth noting that the usefulness of channel mobility as an indicator of performance in aggressively scaled FETs is debatable as devices with channel lengths < 30 nm are going to be strongly limited by contact resistance (including carrier injection efficiency) with minimal dependence on transport in the channel[28,29].

The most representative FET parameters are listed in Table 1 as a suggested reporting checklist. Additional parameters are briefly discussed in Note S4.

Table 1| Checklist of suggested device parameters to report

Name	Characteristics	Additional details
Structural parameters	Contact length, L_c Channel length, L_{ch} Channel width, W_{ch} Insulator thickness, t_{ins} Channel thickness, t_{ch}	Specify contact and gating geometry/materials; include high-resolution electron microscopy evidence when reporting sub-20 nm dimensions (especially for L_c and L_{ch})
Insulator capacitance, C_{ins}	Capacitance-voltage or Capacitance-frequency	Measured C_{ins} is more accurate than estimating ϵ_{ins} especially when a high-*k* insulator is used
Threshold voltage, V_T, and hysteresis, ΔV_T	Extrapolation in the linear portion of the transfer curve[19]	• I_D-V_{GS} should have forward and backward sweeps • Consider V_T uncertainty due to hysteresis (charge trapping), the dependence of V_{DS} and *I-V* sweeps (Note S2)
Drain current in saturation regime, I_{sat}	I_D-V_{DS} (saturation regime)	• Sweep I_D-V_{DS} to saturation regime • Specify carrier density where I_{sat} is extracted • Normalized by channel width
Contact resistance, R_c	TLM[23] (Note S3)	• Linear regime (small V_{DS}) • Specify carrier density n_S or plot R_c vs. n_S • TLM should have at least four channels and include at least one each of contact and channel resistance dominated devices
Conductivity mobility, μ_{con}	$\frac{1}{qn_S R_{sh}}$	• R_{sh} is extracted from the slope of TLM plots or from four-probe measurements[22]. Unit: Ω/square • Carrier density near the source: $n_S \approx C_{ins}V_{OV}/q$ • Mobility from $R_{sh} = (qn_S\mu)^{-1}$ • Plot mobility vs n_S to show field dependence

Transconductance, g_m	Transfer or output curves $g_m = \frac{\partial I_D}{\partial V_{GS}}$ at certain V_{DS}	Specify g_m (linear) or g_m(saturation)
Subthreshold Swing, *SS*	Subthreshold curves (inverse slope in mV/decade below V_T)	• *SS* depends on C_{ins} and interface trap capacitance C_{it} • Plot *SS* vs. $\log_{10}(I_D)$
I_{on}/I_{off}	Subthreshold curves at saturation regime, V_{DS} = V_{DS} (sat)	• Report I_{max}/I_{min} as an alternative along with n_S range • Plot I_G vs V_{GS} to show leakage current
DIBL	ΔV_T / ΔV_{DS} from transfer curves	Key for short-channel devices

Beyond the parameters in Table 1, showing statistics and variation is strongly encouraged to obtain comprehensive coverage of the device performance. The variation can be shown as error bars, box plots, coefficient of variation, or cumulative distribution function (see Note S5 for demonstration). Due to many nonidealities associated with emerging materials or unconventional device geometries, it is almost unavoidable that there could be considerable uncertainties in many extracted parameters, including R_c, n_S, and mobilities. These parameters are often interdependent. Reducing device variation is a major research theme for the eventual application of emergent FETs. Whatever measurements and specific analysis approaches are taken to determine these parameters, the details should be clearly and explicitly reported, and our recommended approaches are demonstrated herein.

Once an emerging FET has been systematically parameterized, benchmarking tables and plots are extremely useful for comparing devices from different reports. Because the electric fields are the driving forces within FETs, benchmarking performance metrics based on electric fields is natural. However, special care is needed in considering electric fields in devices, because they are spatially non-uniform and depend on many other factors, such as fringing fields and quantum capacitance C_q. Thus, the electric fields in nanoscale FETs are more complicated than the simple definition of an applied voltage divided by a physically defined length. For example, it is a reasonable assumption that the channel electric field in the channel, E_{ch} increases linearly from source to drain in the linear region of operation, but E_{ch} peaks sharply at the drain end of the channel in classical pinch-off (saturation)[30]. To account for this, the *average* E_{ch} can be approximated as $(V_{DS} - 2I_{lin}R_c)/L_{ch}$ in the linear regime, accounting for voltage dropped at the contacts.

The vertical electric field at the source end, E_{gate}, can be estimated as V_{OV}/t_{ins} if a planar gate is used. In turn, E_{gate} and the gate insulator permittivity determine the carrier density in the channel. Yet, both E_{gate} and the gate insulator permittivity are rather challenging to measure accurately. One more word of caution is justified: because many low-dimensional materials exhibit a low density of states, C_{ins} needs to be replaced by $C_{ins}C_q/(C_{ins}+C_q)$ where quantum capacitance (C_q) can be approximated as q^2DOS (density of states)[31,32]. Only for $C_{ins} \ll C_q$ this expression becomes equivalent to C_{ins}. Because multiple parameters in Table 1 depend on n_S, benchmarking these versus n_S is recommended to

evaluate devices from different studies. A suggested list of benchmarking plots to evaluate device parameters and performance metrics is given in Table 2.

Table 2| Suggested benchmarking plots for evaluating device performance compared with other FETs

Parameter	Benchmarking Plot	Notes
I_{min} and I_{max}	I_{min} vs. I_{max}	• Specify L_{ch} or L_{ch}/EOT • Ideally specify the carrier density at which I_{max} is extracted (Note S1)
I_{sat}	I_{sat} vs. n_S	Label L_{ch} and t_{ch} to imply channel resistance
I_D	I_D vs. L_{ch}	At certain V_{DS} and n_S (*e.g.*, V_{DS} = 1 V and $n_S = 10^{13}$ cm^{-2})
R_c	R_c vs. n_S	• Or benchmark R_c vs. t_{ch} at certain n_S • Specify if semiconductor in contact regions is gated or not
μ_{con}	μ_{con} vs. t_{ch}	For the same material, a thicker channel could have higher mobility due to less surface scattering
g_m	g_m vs. n_S/L_{ch}	• Since $g_m = \frac{W}{L}\mu C_{ins}V_{ov}$, $g_m \propto C_{ins}V_{ov}/L_{ch}$ • $n_S \approx C_{ins}V_{OV}/q$ near the source end, so $g_m \propto n_S/L_{ch}$
SS	SS vs. C_{ins}	• Larger C_{ins} can yield smaller SS • Identify Schottky barrier branch and thermal branch • Or plot SS vs. L_{ch} to show short-channel robustness • Or plot SS vs $\log_{10}(I_D)$

Drain current is the key output of a FET and is also frequently benchmarked and compared. However, many comparisons are oversimplified and not fairly conducted as the drain current depends on many parameters. As mentioned in Table 2, we recommend benchmarking I_D vs. L_{ch} at certain V_{DS} and n_S values, enabling fair comparison between devices having different channel lengths. On the other hand, if a record I_{sat} is claimed, we recommend benchmarking the maximum I_{sat} vs. n_S because it is a much closer indicator for the eventual drive current and ultimately sets the operating delay of a circuit stage (delay $\tau \propto CV_{DD}/I_{sat}$). As mentioned previously, assuming limited short-channel effects, I_{sat} mainly depends on n_S and not on E_{ch}. Usually, one performance metric depends on multiple parameters; hence, key parameters should be annotated on the benchmarking plot (see Table 2).

Reporting and benchmarking example

To demonstrate reporting and benchmarking based on the principles proposed above, MoS_2 is chosen as the example emerging channel material because it is among the most studied semiconducting nanomaterials in recent years and represents a family of 2D materials that holds promise for future transistor applications. Fig. 2a shows an example transistor based on monolayer (1L) MoS_2 grown by chemical vapor deposition (CVD). The device is top-contacted and back-gated, which is the most

common and convenient FET structure used to explore emergent channel materials. The approach is as follows:

Step 1. The structural parameters of the device are determined and labelled (Fig. 2a). In this example, the gate insulator is AlO_x, which is grown by atomic layer deposition (ALD) with the oxide capacitance ($C_{ins} \approx 280$ nF/cm^2) evaluated from a capacitance-voltage measurement of a large-area test capacitor. The thickness of the oxide ($t_{ins} \approx 20$ nm) is further confirmed by cross-sectional transmission electron microscope (TEM) imaging. From the thickness and capacitance, the dielectric constant of the oxide is estimated to be $\varepsilon_{ins} \approx 6$. Other dimensions such as L_{ch}, W_{ch}, and L_c are confirmed by scanning electron microscopy (SEM) after electrical characterization.

Step 2. I_D-V_{GS} and I_D-V_{DS} characterization are performed, making sure that V_{DS} and V_{GS} are swept high enough for the device to reach saturation, and the V_{GS} sweep range is sufficient to observe I_{min} in both the linear (low V_{DS}) and saturation (high V_{DS}) operation regions. I_{max}/I_{min} of ~4×10^7 at $V_{DS} = 4$ V can be extracted from the subthreshold curve in Fig. 2b. I_{max} is extracted at $n_S \approx 1.4\times10^{13}$ cm^{-2}. I_{min} is extracted under subthreshold conditions, where $V_{GS} < V_T$, yielding a negative V_{OV} and $n_S \approx 0$. The larger hysteresis for $V_{DS} = 4$ V in Fig. 2b,c highlights the impact of the larger source-drain field on the interface charges in the channel. Due to hot-carrier stress from the high V_{DS} (explained later), V_T increases for high V_{DS}, resulting in an extracted DIBL of –274 to –436 mV/V considering the effect of hysteresis. Also, from the transfer curves in Fig. 2c, the maximum g_m(sat) and g_m(lin) are estimated to be ~ 59 µS/µm and ~1.7 µS/µm, respectively. In Fig. 2d, approximate current saturation is observed with I_{sat} around 325 µA/µm obtained at $n_S \approx 1.3\times10^{13}$ cm^{-2} at $V_{DS} = 4$ V. The blue and red shows linear and saturation regions, approximately. The I_D-V_{DS} spacing is sub-linear at the highest V_{GS}, which is a sign of possible self-heating.

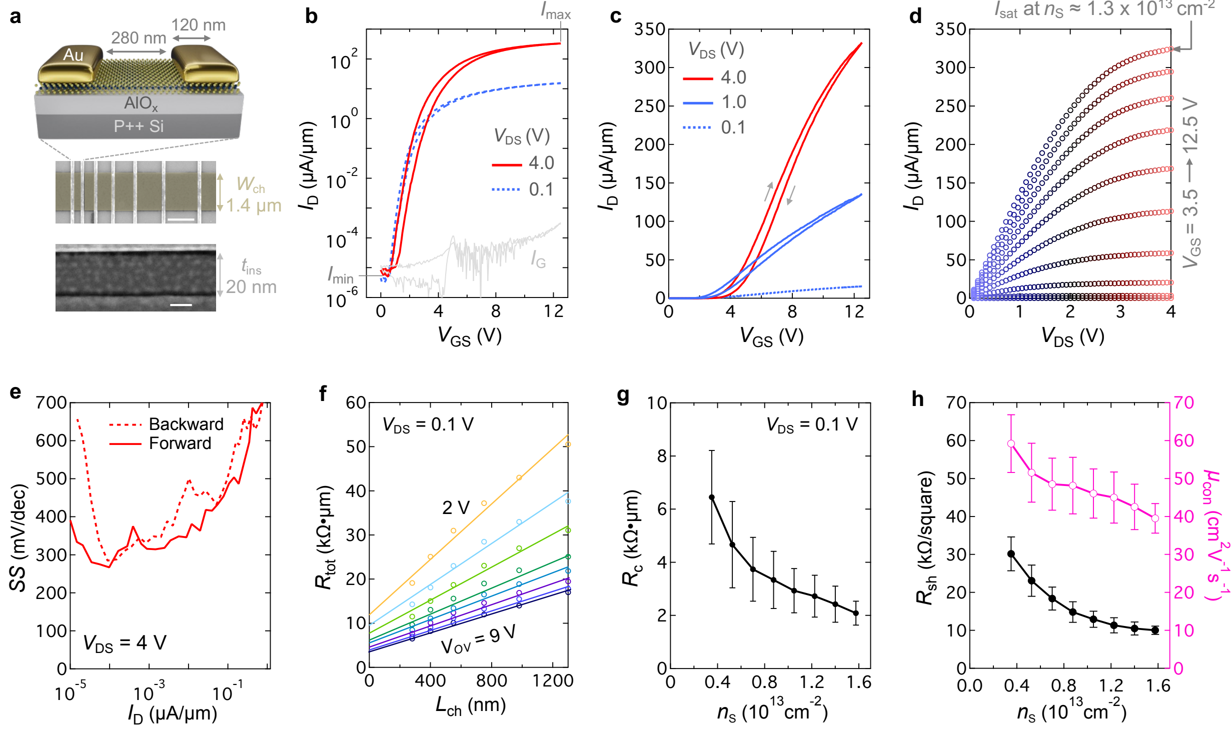

Fig. 2| Example of reporting device performance for monolayer Au-contacted MoS_2 FETs. **a,** Device schematic and the basic structural parameters of the MoS_2 FET. An SEM image of a TLM structure with false-colored MoS_2 area (scale bar, 1 µm) and a cross-section TEM image of the AlO_x (scale bar, 10 nm). **b**, Subthreshold (I_D-V_{GS}) curve of the device with I_{max} and I_{min} labelled. The I_G is the gate leakage current at V_{DS} = 4 V. The curve for V_{DS} = 1 V is intentionally not shown so the plot is less crowded. **c**, Transfer (I_D-V_{GS}) curves of the device showing larger hysteresis with larger V_{DS}. **d**, Output (I_D-V_{DS}) curves of the device. V_{GS} changes in steps of 1 V. **e**, *SS* vs. I_D for both forwards and backwards V_{GS} sweeps in (**b**). **f**, Extraction of R_c from the TLM structure in (**a**). The R_{tot} is extracted at V_{DS} = 100 mV. **g**, Contact resistance vs. n_S showing the contact gating effect that is a result of the device operating as a Schottky barrier transistor with the gate modulating the semiconductor in the source/drain contact regions[33]. **h,** Extracted sheet resistance (left axis) and conductivity mobility (right axis) versus n_S. In **g** and **h**, error bars reflect 90% confidence interval from a least-squares fit of the TLM.

Figures 2a-d are used for primary characterization of one device, and more derived plots are shown in Fig. 2e-h, providing a more complete picture of the device characteristics. The device spread and parameter variations based on ten similar TLM structures are shown in Fig. S5. The full range of *SS* vs. I_D is plotted in Fig. 2d, with a minimum *SS* of 280 mV/dec extracted in the subthreshold regime. Additionally, because V_T depends on V_{DS}, it is key to extract V_T at the associated V_{DS} (as noted in Table 1). R_c, R_{sh}, and subsequently μ_{con} are extracted by using a TLM structure as shown in Fig. 2f-h. The R_c is estimated to be around 2.1 kΩ·µm, which is comparable to the R_{ch} of 2.8 kΩ·µm for the device with channel length of 280 nm. The relation between n_S and extracted R_c is plotted in Fig. 2g to show the effect of the overall back gate on the contact resistance (i.e., contact gating[33–35]). Fig. 2h shows

μ_{con} decreases from 59 to 40 $cm^2V^{-1}s^{-1}$ with increasing n_S, likely due to the increased electron scattering with the oxide surface roughness.

Step 3: As a simplified example, we benchmark key device performance parameters in Fig. 3 with a limited number of reports included. Currently, most papers do not report I_D-V_{GS} at V_{DS} (sat) or close to V_{DD} as recommended above. Hence, plotting I_{min} vs. I_{max} at certain V_{DS} (*e.g.*, V_{DS} = 1 V) while annotating L_{ch} is an acceptable approach (Fig. 3a). The upper limit of the carrier density is set at $n_S = 10^{13}$ cm^{-2}, ensuring a fair comparison of $I_{max.}$ The I_{max}/I_{min} ratio annotated on the right axis is also shown in the dashed lines in Fig. 3a. Due to a better electrostatic control from the gate, devices with a larger L_{ch}/EOT ratio tend to yield a higher I_{max}/I_{min} (where EOT is the equivalent oxide thickness). Other parameters also play a role such as the leakage currents through the gate insulator or from source to drain. Large channel width can also produce a more accurate width-normalized I_{min}, especially when I_{min} is below the instrument noise floor. For example, Illarionov *et al.*[36] demonstrated a relatively high I_{max}/I_{min} ratio in devices with a 20 µm channel width. Further study is still needed to investigate how to achieve high I_{max} and small I_{min} in aggressively scaled devices (small L_{ch}, L_c, and EOT).

As mentioned previously, a high drain current in the saturation regime is a key performance metric. In Fig. 3b, I_{sat} is plotted versus n_S from representative studies of FETs based on MoS_2 as the channel material. We note that the I_{sat} is extracted at different V_{DS} because different devices have different channel lengths, as annotated in Fig. 3b. We caution against plotting I_{sat}/L_{ch} vs. n_S because it implies that L_{ch} is the main limiting factor for I_{sat}, which is not necessarily true, especially for scaled devices where contact resistance typically dominates I_{sat} performance. Importantly, it is clear that I_{sat} needs to be further improved to meet the high-performance target of the most recent technology guidelines (at $V_{DD} \approx 0.65$ V near 2030)[37]. Many reports already used high n_S but fell short on I_{sat} even with channel lengths down to ~10 nm[38], being strongly limited by their contacts.

Recently, semimetal contacts such as bismuth have been shown to produce high-quality contacts[39]. It is nevertheless noteworthy that the two Bi-1L MoS_2 devices have a wide range of I_{sat} performance, encompassing all the other devices in Fig. 3b, yet the channel length difference between the two devices is only 115 nm. Interestingly, one of the Bi-contacted devices (L_{ch} = 150 nm) actually underperforms other Au-contacted devices with longer channel lengths. Hence, although some approaches show potential to achieve the International Roadmap for Devices and Systems (IRDS) high-performance goal of I_{sat} for the post-2030 era[37], further investigation is still needed to reliably and reproducibly realize high I_{sat} from a monolayer channel. In next-generation FETs, I_{sat} could also be

increased by shifting to nanosheet device designs, which stack multiple channels vertically to improve current density in the same device footprint[40].

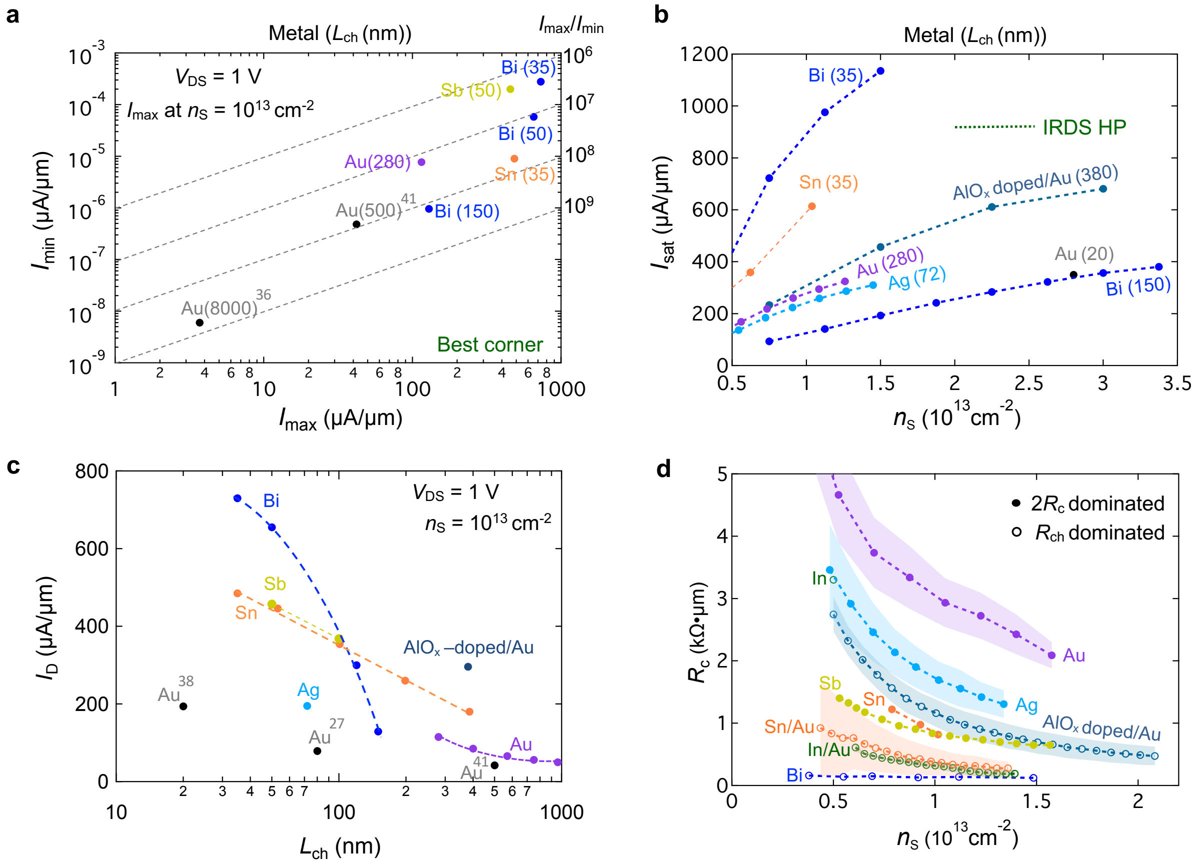

Fig. 3 | Example Benchmarking device performance of monolayer MoS_2 FETs. **a**, Benchmarking I_{min} vs. I_{max}. The I_{max} is extracted at $n_S = 10^{13}$ cm^{-2}. For simplicity, the I_{min} of the data points are extracted at their respective smallest current. More rigorous benchmarking of I_{min} vs I_{max} is in Note S1. **b**, Benchmarking I_{sat} versus n_S, where the channel length in nm is labelled next to the contact metals used in the devices. I_{sat} are extracted at different V_{DS} (listed in Table 3). These devices do not have the same V_{DS}(sat) as devices with different channel lengths and saturate at different V_{DS}. The IRDS HP is shown in a range of n_S to represent uncertainties of the carrier density in future generation technologies. **c**, Benchmarking I_D versus L_{ch} at V_{DS} = 1 V and $n_S = 10^{13}$ cm^{-2}. Ref. [41] uses top-gate, while other reports use back-gate. **d**, Benchmarking R_c versus n_S in a few representative reports. The shaded regions represent uncertainties reported in the respective studies (Ag[14] uses 95% confidence interval, while In/Au[42], Sn/Au[42], and Au use standard error from the linear regression of TLM). The R_c vs. n_S of Sb[43] is obtained from Y-function method. The filled and open symbol show that the shortest channel device in the TLM structure is $2R_c$ and R_{ch} dominated, respectively. If R_{ch} dominates or the R_c is over an order of magnitude smaller than the R_{tot} for the smallest device in TLM, the extracted R_c is of questionable validity; i.e., solid symbol data is more reliable per Note S3. Different colors are assigned to different reported devices. The purple Au data denote devices in Fig. 2. Most of the data are extracted from published reports: Ag[14], AlO_x doped/Au[15], In/Au[42], Sn/Au[42], Sb[43], In[44] and Sn[45]. In **a** and **c**, reference numbers are added for Au-contacted devices to better differentiate their performance. A few studies are plotted as dotted lines to highlight the trends and to improve the clarity of the plots.

In some reports, a proper saturation current is not given. Also, since different devices use different channel lengths, I_{sat} is often extracted at different V_{DS}. To highlight the impact of channel length, we recommend benchmarking I_D vs. L_{ch} at V_{DS} = 1 V and $n_S = 10^{13}$ cm^{-2}. This plot enables a direct comparison of devices with similar L_{ch}. In Fig. 3c, with channel length decreasing from 200 nm to 38 nm, both Bi[39] and Sn[45] contacted devices yield relatively large increases in drain current. We note that the Bi-contacted devices are based on different MoS_2 films. The different quality of the MoS_2 may partially contribute to the large increase of I_D with a relatively small change in L_{ch}. Nevertheless, Figures 3c,d present the potential of atomic thin materials for producing high drain current, especially for scaled devices.

In Fig. 3d, R_c is plotted against n_S considering most devices have gated contacts (i.e., the back-gate modulates the channel and contacts[33–35]). While some reported R_c values reach below 500 Ω·µm, their TLM extractions are all based on channel resistance-dominated devices, which can lead to questionable validity in their claimed R_c (an artificially small or even a negative R_c can be extracted, see Note S3 for details). We advocate that if a record R_c is claimed from TLM, R_{sh} should be cross-examined by using other methods such as four-probe measurements, which can provide a relatively accurate estimation of R_{sh} vs. n_S (Note S3). With R_{sh} vs. n_S from four-probe measurements, R_c vs. n_S can be derived by deducting the $R_{ch} = R_{sh}L_{ch}$ from R_{tot} to confirm the TLM extracted value. Showing extraction of R_c from many TLM structures can also increase confidence in the data by providing an average value of the R_c rather than just the minimal value from a single TLM[46,47]. Furthermore, R_c is heavily impacted by contact gating, as evident from the similar trends of R_c vs. n_S observed in different studies; therefore, further research is needed to obtain a small R_c without gating the contacts.

Looking forward, many opportunities remain to develop transistors that simultaneously have small contact resistance, high I_{sat}, large I_{max}/I_{min} ratio, and minimal short-channel effects by using emergent nanomaterials. To achieve this technological goal, interface engineering at the contacts and gate dielectric needs to be further investigated[48–50], along with progress in material synthesis[51] and integration[52]. Moreover, it is important to focus on channel thicknesses below ~3 nm, where low-dimensional nanomaterials can excel compared to Si, which suffers from poor carrier transport properties and a widened band gap in this thickness regime[53].

In addition to the example benchmarking plots in Fig. 3, other benchmarks can also be used to compare different devices. For example, as included in Table 2, plotting I_{max}/I_{min} vs. t_{ch} or I_{max}/I_{min} vs. L_{ch}/EOT to compare the off-state device performance. Plotting SS vs. C_{ins} or SS vs. $\log_{10}(I_D)$[54] can be used to evaluate subthreshold behaviour and trends across different devices. Finally, to show the

quality of the channel materials, the channel sheet resistance or conductivity mobility can be plotted vs. carrier densities, as in Fig. 2h. Representative reports with relatively large I_{sat} are listed in Table S1, including results for FETs with both monolayer and multilayer MoS_2 channels (example benchmarking plots in Note S6). In the literature, notable benchmarking examples can be found in Refs.[39,55] that highlight different channel materials, and in Ref. [56] that focuses on device performance in integrated circuits (speed, gain, density, power consumption, and fan-out capabilities, etc.).

Conclusions

Our guidelines should help put key performance metrics in a proper context and enable researchers to effectively report and benchmark emergent transistors based on various emergent nanomaterials. While each of the listed metrics is significant, it is not necessary — nor always possible — to extract and present all of them. As such, it is essential to completely describe the device geometry, to collect and report appropriate current-voltage characteristics, and to describe in detail the procedures followed in the experiments. The approaches used to analyze data and extract benchmarking metrics should also be described in detail. Depending on the context and need, we recommend three sets of parameters to report and benchmark. The first includes maximum saturation current, on/off-current ratio, transconductance, and subthreshold swing. These values can be directly obtained from the measured *I-V* characteristics that cover both linear and saturation regimes. These values are mainly determined by the intrinsic material properties, gate stack configuration, and contact quality. The second includes the derived parameters such as mobilities and contact resistance, where uncertainty and statistical spread on these derived parameters should be shown. The third set of parameters are those specific to certain transistor demonstrations based on the target application[57,58]. For example, DIBL is essential when reporting and evaluating ultra-scaled FETs. It is important — whenever possible — to benchmark against other novel materials and also state-of-the-art in mature technology[39,55]. By using these guidelines, it should be possible to comprehensively and consistently reveal, highlight, discuss, compare, and evaluate device performance, thus helping to identify advances and opportunities in the search for improved transistors.

References

1. Chen, Z. *et al.* An integrated logic circuit assembled on a single carbon nanotube. *Science* **311**, 1735 (2006).
2. Franklin, A. D. *et al.* Sub-10 nm carbon nanotube transistor. *Nano Lett.* **12**, 758–762 (2012).
3. Geim, A. K. Graphene: Status and prospects. *Science* **324**, 1530–1534 (2009).
4. Ye, P. D. *et al.* Phosphorene An Unexplored 2D Semiconductor with a High Hole Mobility. *ACS Nano* **8**, 4033–4041 (2014).
5. Tao, L. *et al.* Silicene field-effect transistors operating at room temperature. *Nat. Nanotechnol.* **10**,

227–231 (2015).
6. Wang, Y. *et al.* Field-effect transistors made from solution-grown two-dimensional tellurene. *Nat. Electron.* **1**, 228–236 (2018).
7. Radisavljevic, B., Radenovic, A., Brivio, J., Giacometti, V. & Kis, A. Single-layer MoS_2 transistors. *Nat. Nanotechnol.* **6**, 147–150 (2011).
8. Das, S., Chen, H. Y., Penumatcha, A. V. & Appenzeller, J. High performance multilayer MoS_2 transistors with scandium contacts. *Nano Lett.* **13**, 100–105 (2013).
9. English, C. D., Shine, G., Dorgan, V. E., Saraswat, K. C. & Pop, E. Improved Contacts to MoS_2 Transistors by Ultra-High Vacuum Metal Deposition. *Nano Lett.* **16**, 3824–3830 (2016).
10. Sirringhaus, H. 25th Anniversary Article: Organic Field-Effect Transistors: The Path Beyond Amorphous Silicon. *Adv. Mater.* **26**, 1319–1335 (2014).
11. Waldrip, M., Jurchescu, O. D., Gundlach, D. J. & Bittle, E. G. Contact Resistance in Organic Field-Effect Transistors: Conquering the Barrier. *Adv. Funct. Mater.* **30**, 1904576 (2020).
12. Li, S. *et al.* Nanometre-thin indium tin oxide for advanced high-performance electronics. *Nat. Mater.* **18**, 1091–1097 (2019).
13. Li, M. Y., Su, S. K., Wong, H. S. P. & Li, L. J. How 2D semiconductors could extend Moore’s law. *Nature* **567**, 169–170 (2019).
14. Smithe, K. K. H., English, C. D., Suryavanshi, S. V. & Pop, E. High-Field Transport and Velocity Saturation in Synthetic Monolayer MoS_2. *Nano Lett.* **18**, 4516–4522 (2018).
15. McClellan, C. J., Yalon, E., Smithe, K. K. H., Suryavanshi, S. V. & Pop, E. High Current Density in Monolayer MoS_2 Doped by AlO_x. *ACS Nano* **15**, 1587–1596 (2021).
16. Datye, I. M. *et al.* Reduction of hysteresis in MoS_2 transistors using pulsed voltage measurements. *2D Mater.* **6**, 011004 (2019).
17. Streetman, B. G. & Banerjee, S. K. *Solid State Electronic Devices, 6th Edition*. (Pearson, 2006).
18. Pinckney, N. *et al.* Impact of FinFET on near-threshold voltage scalability. *IEEE Des. Test* **34**, 31–38 (2017).
19. Ortiz-Conde, A. *et al.* A review of recent MOSFET threshold voltage extraction methods. *Microelectron. Reliab.* **42**, 583–596 (2002).
20. Ghibaudo, G. New method for the extraction of MOSFET parameters. *Electron. Lett.* **24**, 543–545 (1988).
21. Chang, H. Y., Zhu, W. & Akinwande, D. On the mobility and contact resistance evaluation for transistors based on MoS_2 or two-dimensional semiconducting atomic crystals. *Appl. Phys. Lett.* **104**, 113504 (2014).
22. Pang, C. *et al.* Mobility Extraction in 2D Transition Metal Dichalcogenide Devices—Avoiding Contact Resistance Implicated Overestimation. *Small* **17**, 2100940 (2021).
23. Schroder, D. K. *Semiconductor Material and Device Characterization, 3rd Edition*. (Wiley-IEEE Press, 2015).
24. Mleczko, M. J. *et al.* $HfSe_2$ and $ZrSe_2$: Two-dimensional semiconductors with native high-k oxides. *Sci. Adv.* **3**, e1700481 (2017).
25. Nasr, J. R., Schulman, D. S., Sebastian, A., Horn, M. W. & Das, S. Mobility Deception in Nanoscale Transistors: An Untold Contact Story. *Adv. Mater.* **31**, 1806020 (2019).
26. Bittle, E. G., Basham, J. I., Jackson, T. N., Jurchescu, O. D. & Gundlach, D. J. Mobility overestimation due to gated contacts in organic field-effect transistors. *Nat. Commun.* **7**, 10908 (2016).
27. Smithe, K. K. H., English, C. D., Suryavanshi, S. V. & Pop, E. Intrinsic electrical transport and performance projections of synthetic monolayer MoS_2 devices. *2D Mater.* **4**, 011009 (2017).
28. Franklin, A. D. Nanomaterials in transistors: From high-performance to thin-film applications. *Science* **349**, (2015).
29. Das, S. *et al.* Transistors based on two-dimensional materials for future integrated circuits. *Nat. Electron. 2021 411* **4**, 786–799 (2021).
30. Pao, H. C. & Sah, C. T. Effects of diffusion current on characteristics of metal-oxide (insulator)-

semiconductor transistors. *Solid State Electron.* **9**, 927–937 (1966).
31. John, D. L., Castro, L. C. & Pulfrey, D. L. Quantum capacitance in nanoscale device modeling. *J. Appl. Phys.* **96**, 5180 (2004).
32. Xu, H., Zhang, Z. & Peng, L.-M. Measurements and microscopic model of quantum capacitance in graphene. *Appl. Phys. Lett.* **98**, 133122 (2011).
33. Appenzeller, J., Zhang, F., Das, S. & Knoch, J. Transition metal dichalcogenide schottky barrier transistors: A device analysis and material comparison. in *2D Materials for Nanoelectronics* (eds. Houssa, M., Dimoulas, T. & Molle, A.) 207–240 (CRC Press, 2016).
34. Arutchelvan, G. *et al.* From the metal to the channel: A study of carrier injection through the metal/2D MoS_2 interface. *Nanoscale* **9**, 10869–10879 (2017).
35. Prakash, A., Ilatikhameneh, H., Wu, P. & Appenzeller, J. Understanding contact gating in Schottky barrier transistors from 2D channels. *Sci. Rep.* **7**, 12596 (2017).
36. Illarionov, Y. Y. *et al.* Improved Hysteresis and Reliability of MoS_2 Transistors with High-Quality CVD Growth and Al_2O_3 Encapsulation. *IEEE Electron Device Lett.* **38**, 1763–1766 (2017).
37. IEEE International Roadmap for Devices and Systems. https://irds.ieee.org/ (2020).
38. Patel, K. A., Grady, R. W., Smithe, K. K. H., Pop, E. & Sordan, R. Ultra-scaled MoS_2 transistors and circuits fabricated without nanolithography. *2D Mater.* **7**, 015018 (2020).
39. Shen, P.-C. *et al.* Ultralow contact resistance between semimetal and monolayer semiconductors. *Nature* **593**, 211–217 (2021).
40. Ahmed, Z. *et al.* Introducing 2D-FETs in device scaling roadmap using DTCO. in *International Electron Devices Meeting, IEDM* 22.5.1-22.5.4 (2020). doi:10.1109/IEDM13553.2020.9371906.
41. Lembke, D. & Kis, A. Breakdown of High-Performance Monolayer MoS_2 Transistors. *ACS Nano* **6**, 10070–10075 (2012).
42. Kumar, A. *et al.* Sub-200 $\Omega\cdot\mu m$ Alloyed Contacts to Synthetic Monolayer MoS_2. in *IEEE International Electron Devices Meeting (IEDM)* 154–157 (2021).
43. Chou, A. *et al.* Antimony Semimetal Contact with Enhanced Thermal Stability for High Performance 2D Electronics. in *IEEE International Electron Devices Meeting (IEDM)* 150–153 (2021).
44. Wang, Y. *et al.* Van der Waals contacts between three-dimensional metals and two-dimensional semiconductors. *Nature* **568**, 70–74 (2019).
45. Chou, A. S. *et al.* High On-State Current in Chemical Vapor Deposited Monolayer MoS_2 nFETs with Sn Ohmic Contacts. *IEEE Electron Device Lett.* **42**, 272–275 (2021).
46. Sebastian, A., Pendurthi, R., Choudhury, T. H., Redwing, J. M. & Das, S. Benchmarking monolayer MoS_2 and WS_2 field-effect transistors. *Nat. Commun.* **12**, 693 (2021).
47. Kumar, A., Tang, A., Philip Wong, H. S. & Saraswat, K. Improved Contacts to Synthetic Monolayer MoS2 – A Statistical Study. in *IEEE International Interconnect Technology Conference* (IEEE, 2021). doi:10.1109/IITC51362.2021.9537515.
48. Cheng, Z., Price, K. & Franklin, A. D. Contacting and Gating 2-D Nanomaterials. *IEEE Trans. Electron Devices* **65**, 4073–4083 (2018).
49. Illarionov, Y. Y. *et al.* Insulators for 2D nanoelectronics: the gap to bridge. *Nat. Commun. 2020 111* **11**, 1–15 (2020).
50. Cheng, Z. *et al.* Are 2D Interfaces Really Flat? *ACS Nano* **16**, 5316–5324 (2022).
51. Zhou, J. *et al.* A library of atomically thin metal chalcogenides. *Nat. 2018* **556**, 355–359 (2018).
52. Liu, Y. *et al.* Van der Waals heterostructures and devices. *Nat. Rev. Mater.* **1**, 16042 (2016).
53. Uchida, K., Koga, J. & Takagi, S. Experimental study on electron mobility in ultrathin-body silicon-on-insulator metal-oxide-semiconductor field-effect transistors. *J. Appl. Phys.* **102**, 074510 (2007).
54. Haratipour, N., Namgung, S., Oh, S. H. & Koester, S. J. Fundamental Limits on the Subthreshold Slope in Schottky Source/Drain Black Phosphorus Field-Effect Transistors. *ACS Nano* **10**, 3791–3800 (2016).
55. Liu, Y. *et al.* Promises and prospects of two-dimensional transistors. *Nature* **591**, 43–53 (2021).

56. Nikonov, D. E. & Young, I. A. Benchmarking of Beyond-CMOS Exploratory Devices for Logic Integrated Circuits. *IEEE J. Explor. Solid-State Comput. Devices Circuits* **1**, 3–11 (2015).
57. Abuzaid, H., Williams, N. X. & Franklin, A. D. How good are 2D transistors? An application-specific benchmarking study. *Appl. Phys. Lett.* **118**, 030501 (2021).
58. Lemme, M. C., Akinwande, D., Huyghebaert, C. & Stampfer, C. 2D materials for future heterogeneous electronics. *Nat. Commun. 2022 131* **13**, 1–5 (2022).

---

[1]Nanoscale Device Characterization Division, National Institute of Standards and Technology, Gaithersburg, MD 20899, USA. [2]Department of Electrical and Computer Engineering, Purdue University, West Lafayette, IN 47907, USA. [3]Department of Chemistry and Biochemistry, University of California, Los Angeles, Los Angeles, CA 90095, USA. [4]Theiss Research, La Jolla, CA 92037, USA. [5]School of Integrated Circuits, Peking University, Beijing 100871, China. [6]Electrical and Computer Engineering, New York University, Brooklyn, NY 11201, USA. [7]Center for Quantum Phenomena, Physics Department, New York University, New York, NY 10003, USA. [8]IMEC, Leuven, Belgium. [9]RWTH Aachen University, Chair of Electronic Devices, Otto-Blumenthal-Str. 2, Aachen 52074, Germany. [10]AMO GmbH, Advanced Microelectronic Center Aachen, Otto-Blumenthal-Str. 25, Aachen, 52074 Germany. [11]Key Laboratory for the Physics and Chemistry of Nanodevices and Center for Carbon-based Electronics, Department of Electronics, Peking University, Beijing, China. [12]Department of Electrical and Computer Engineering, University of Minnesota, Minneapolis, MN 55455 USA. [13]Department of Electrical Engineering, Stanford University, Stanford, CA 94305, USA. [14]Department of Electrical and Computer Engineering, Duke University, Durham, NC 27708, USA. [15]Department of Chemistry, Duke University, Durham, NC 27708, USA. †: corresponding authors.

Acknowledgements

We acknowledge Dr. Huairuo Zhang and Dr. Albert Davydov from the National Institute of Standards and Technology for their help on the TEM images of the oxide in Fig. 2. We acknowledge Dr. Guoqing Li and Prof. Linyou Cao from North Carolina State University for providing the CVD MoS_2 film. This work is supported by NEWLIMITS, a center in nCORE, a Semiconductor Research Corporation (SRC) program sponsored by NIST through award number 70NANB17H041. A.D.F acknowledges the support from the National Science Foundation under Grant ECCS 1915814. M.C.L. acknowledges funding from the European Union's Horizon 2020 research and innovation program under grant agreements 881603 (Graphene Flagship), 952792 (2D-EPL) and 829035 (QUEFORMAL), as well as the Deutsche Forschungsgemeinschaft (DFG, German Research Foundation) through the grants LE 2440/7-1 and LE 2440/8-1. Furthermore, support by the Bundesministerium für Bildung und Forschung (BMBF, German Ministry of Education and Research) through the grants 03XP0210 (GIMMIK) and 03ZU1106 (NeuroSys) is acknowledged. L.-M.P. acknowledges the National Science Foundation of China under the grant 61888102. S.J.K. acknowledges support from the NSF through award no. DMR-1921629. Fabrication and measurements were partially performed at the NIST Center for Nanoscale Science and Technology and at Duke Shared Manufacturing and Instrument Facility (SMIF).

Author contributions

All authors contributed to the preparation of the manuscript.

Notes

The authors declare no competing financial interest.

Certain commercial equipment, instruments, or materials are identified in this paper to specify the experimental procedure adequately. Such identifications are not intended to imply recommendation or endorsement by the National Institute of Standards and Technology (NIST), nor it is intended to imply that the materials or equipment identified are necessarily the best available for the purpose.

Corresponding authors

Zhihui Cheng, zhihui.cheng@alumni.duke.edu

Aaron D. Franklin, aaron.franklin@duke.edu

Curt A. Richter, curt.richter@nist.gov

Data availability

The data used in the paper are available from the corresponding authors upon reasonable request.

Supplementary Information for

How to Report and Benchmark Emerging Field-Effect Transistors

Zhihui Cheng[1,2,†], Chin-Sheng Pang[2], Peiqi Wang[3], Son T. Le[1,4], Yanqing Wu[5], Davood Shahrjerdi[6,7], Iuliana Radu[8], Max C. Lemme[9,10], Lian-Mao Peng[11], Xiangfeng Duan[3], Zhihong Chen[2], Joerg Appenzeller[2], Steven J. Koester[12], Eric Pop[13], Aaron D. Franklin[14,15,†], Curt A. Richter[1,†]

[1]Nanoscale Device Characterization Division, National Institute of Standards and Technology, Gaithersburg, MD 20899, USA. [2]Department of Electrical and Computer Engineering, Purdue University, West Lafayette, IN 47907, USA. [3]Department of Chemistry and Biochemistry, University of California, Los Angeles, Los Angeles, CA 90095, USA. [4]Theiss Research, La Jolla, CA 92037, USA. [5]School of Integrated Circuits, Peking University, Beijing 100871, China. [6]Electrical and Computer Engineering, New York University, Brooklyn, NY 11201, USA. [7]Center for Quantum Phenomena, Physics Department, New York University, New York, NY 10003, USA. [8]IMEC, Leuven, Belgium. [9]RWTH Aachen University, Chair of Electronic Devices, Otto-Blumenthal-Str. 2, Aachen 52074, Germany. [10]AMO GmbH, Advanced Microelectronic Center Aachen, Otto-Blumenthal-Str. 25, Aachen, 52074 Germany. [11]Key Laboratory for the Physics and Chemistry of Nanodevices and Center for Carbon-based Electronics, Department of Electronics, Peking University, Beijing, China. [12]Department of Electrical and Computer Engineering, University of Minnesota, Minneapolis, MN 55455 USA. [13]Department of Electrical Engineering, Stanford University, Stanford, CA 94305, USA. [14]Department of Electrical and Computer Engineering, Duke University, Durham, NC 27708, USA. [15]Department of Chemistry, Duke University, Durham, NC 27708, USA. †: corresponding authors.

Note S1: Rigorously reporting and benchmarking I_{max}/I_{min}

Note S2: Different methods to extract threshold voltage V_T and its uncertainties

Note S3: Extracting R_c from TLM

Note S4: Additional Parameters

Note S5: Demonstration of device spread and parameter variations

Note S6: Benchmarking devices with different channel thicknesses

Note S1: Rigorously reporting and benchmarking I_{max}/I_{min}

The I_{max}/I_{min} ratio is the most-used figure of merit for evaluating off-state performance of a transistor and it depends on multiple factors. First, I_{max}/I_{min} is impacted by material properties such as material quality, bandgaps, and doping conditions. Secondly, the specific device structure and geometry, including the channel length and gate capacitance, also affect the achievable I_{max}/I_{min}. Thirdly, the same device operating at different operation regimes might also have different I_{max}/I_{min}. Combined with the absence of a well-defined V_{DD}, these factors make rigorous reporting and benchmarking guidelines strongly desired for I_{max}/I_{min}. Rigorously reporting I_{max}/I_{min} involves clearly identifying the V_{DS} and V_{GS} values at which the I_{max} and I_{min} are extracted. This practice will help fairly benchmark I_{max}/I_{min} between different devices.

Similar to Fig. 3a, Fig. S1a represents benchmarking I_{max}/I_{min} at $V_{DS} = 1$ V, which is a commonly used bias condition when obtaining subthreshold curves. Under $V_{DS} = 1$ V, short-channel devices (e.g., Device A) may operate at the saturation regime, whereas long-channel devices (e.g., Device B) at the linear regime. While using the same $V_{DS} = 1$ V is a convenient and simple method, the I_{max}/I_{min} likely represent different operation regimes for the two example devices. For a more precise comparison, instead of extracting the I_{max} and I_{min} at the same V_{DS} value for the different devices, it is possible to ensure they are extracted in the same regime (linear or saturation) by using the drain-source electric field instead of V_{DS}; e.g., $E_{DS} = 0.1$ V/µm for the linear regime. This improved comparison is demonstrated in Fig. S1b, where the carrier density at which the I_{max} is extracted is also labeled.

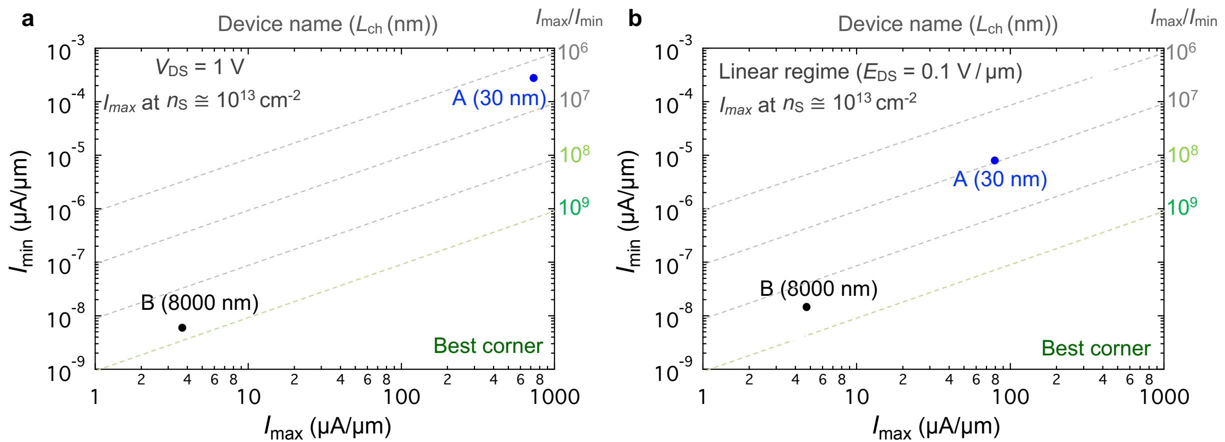

Fig. S1 | Rigorously benchmarking I_{max}/I_{min}. **a**, Benchmarking I_{max}/I_{min} at $V_{DS} = 1$ V, similar to Fig. 3a. Devices A and B are not actual experimental data and are used to demonstrate benchmarking devices with different channel lengths. The carrier densities at which the I_{max} and I_{min} are extracted are also labeled. **b**, Benchmarking I_{max}/I_{min} at the same operation regime, which is the linear regime with drain-to-source field $E_{DS} = 0.1$ V/µm used as an example. Note, the diagonal dashed lines indicate certain values of I_{max}/I_{min}.

Additional factors can impact I_{max}/I_{min} ratio. When benchmarking devices with the same channel material but with different channel thicknesses, plotting I_{max}/I_{min} vs. t_{ch} is suggested. It is noteworthy

that I_{max}/I_{min} also depends on channel length and the equivalent oxide thickness (EOT) of the gate insulator. When the devices to be benchmarked have the same channel thickness, then benchmarking I_{max}/I_{min} vs. L_{ch}/EOT should be considered. In addition, I_{min} can be limited by the measurement instrumentation, especially in materials with larger band gap such as monolayer TMDs. Additional factors impacting I_{max}/I_{min} include contact resistance (which limits I_{max}), leakage currents (which dominate I_{min}) and parasitic capacitances (which affect electrostatic control of the gate), etc.

Note S2: Different methods to extract threshold voltage V_T and its uncertainties

Different methods to extract V_T

A standard method to extract the V_T is not yet available. Refs. [4–7] have investigated and compared different V_T extraction methods. Specifically, in Ref. [4], the authors investigated eleven approaches to extract the V_T and found that similar V_T values in the linear regime can be extracted. In Refs. [5,6], the authors proposed the Y-function method to eliminate the R_c effect when evaluating mobility values. In their studies, the V_T is extracted from the $I_D/g_m^{0.5}$ curve.

Uncertainty of V_T induced by I-V sweeps

The threshold voltage V_T uncertainties can propagate to the estimation of carrier density. Fig. S2 shows an example of V_T shift due to different sweeps (I_D-V_{GS} vs. I_D-V_{DS}) on the same device illustrated in Fig. 2c.

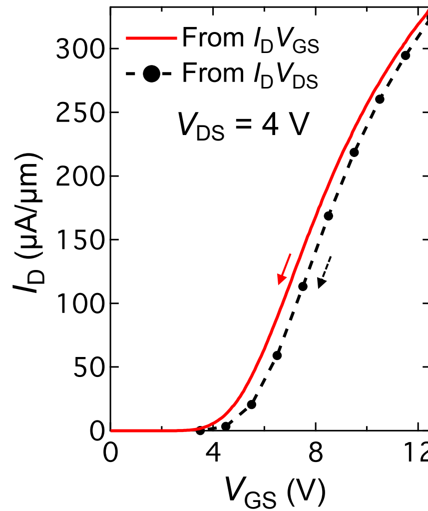

Fig. S2 | Comparison of transfer curves at $V_{DS} = 4$ V from I_D-V_{GS} sweep (red) and extraction from I_D-V_{DS} sweeps (black) based on data in Figures 2b,d of the main text. The direction of the sweeps is the same (backward). A V_T shift of ~0.6 V is observed comparing the I_D-V_{GS} and I_D-V_{DS} sweeps. We presume this shift arises from hot-carrier stress during the I_D-V_{DS} sweeping at high V_{DS} and V_{GS}. Due to high electric fields, energetic electrons become trapped in the gate oxide as fixed charges[8], increasing the V_T. This phenomenon highlights the dependence of V_T on I_D-V_{DS} sweeping.

Note S3: Extracting R_c from TLM

Extracting R_c from TLM data can lead to significant uncertainties. As a reminder, TLM data is a plot of the total resistance (R_{tot}) from a set of devices having all things consistent with their structure and materials except their channel length. TLM data is plotted as R_{tot} vs L_{ch}, where the $R_{tot} = R_{ch} + 2R_c = R_{sh}L_{ch} + 2R_c$, which means when the channel length is zero (y-axis intercept) $R_{tot} = 2R_c$. A reliable R_c must be derived from TLM data that includes devices in the short-channel limit, where **R_c dominates the total resistance** or at least is comparable to the R_{ch}. Ideally, the sheet resistance and its variation need to be sufficiently small; otherwise, a small variation in R_{sh} could lead to substantial errors in R_c. Three examples of TLM data are presented in Fig. S3a, all claiming an R_c of 500 Ω·µm, based on the intercepts to the R_{tot} axis. However, due to the larger R_{sh}, the uncertainty of R_c in TLM A is significantly larger than TLM B (e.g., a small change in R_{sh} for TLM A would result in a large change in the extracted R_c). In TLM A, the shortest channel device has an R_{tot} of 10 kΩ·µm, which is much larger than the claimed R_c of 500 Ω·µm, whereas in TLM B, the R_{tot} is 2 kΩ·µm and the claimed R_c is 500 Ω·µm. As noted above, with a slight variation in the R_{sh} in TLM A, the R_c might be extracted as a very small (and often untrue) value or even a negative value.

Hence, it is critical to have both of the following in a TLM: 1) devices with channel length small enough to ensure $2R_c$ dominates R_{tot} and 2) a sufficient number of longer channel length devices to ensure a reliable R_{sh} extraction based on a linear fit. Another possible scenario to avoid is illustrated with TLM C, which represents a TLM data set where all of the devices are $2R_c$ dominated thus leading to an inaccurate estimation of R_{sh}. This comparison further highlights the need for proper TLM data; as a summary, a valid TLM data set should have at least four channels and include at least one each of contact and channel resistance-dominated devices.

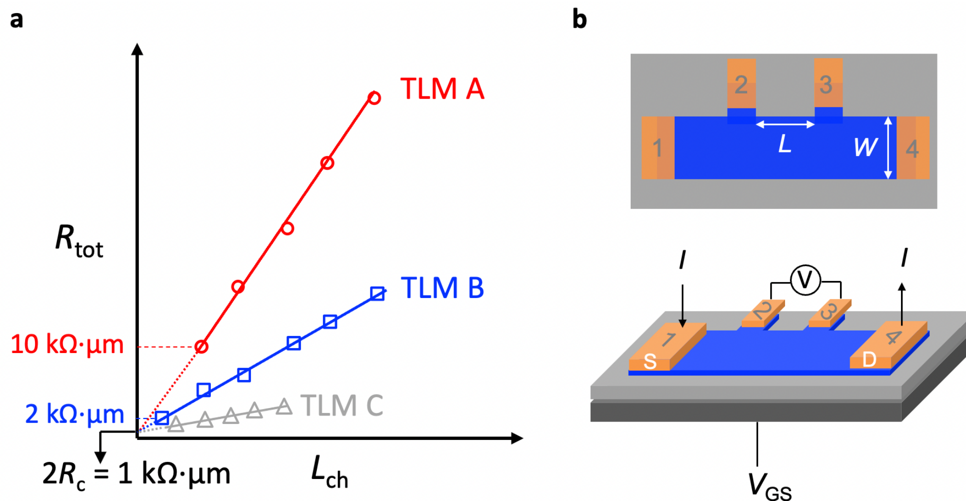

Fig. S3 | a, Demonstration of TLM data sets with all R_{ch}-dominant devices (TLM A, leading to unreliable R_c extraction), all R_c-dominant devices (TLM C, leading to unreliable R_{sh} extraction), and an appropriate balance of devices (TLM B). **b**, Example diagram of four-probe measurements to extract R_{sh}, with a back-gate as a demonstration. The channel resistance R_{ch} between probe 2 and 3 is $R_{14,23} = V_{23}/I_{14}$, where I_{14} is the current flowing from probe 1 to 4 and V_{23} is the voltage between probe 2 and 3. $R_{sh} = R_{14,23}\,(W/L)$. R_{sh} can be obtained while V_{GS} is swept, yielding R_{sh} vs. V_{GS} or carrier density, which can be used to cross-examine the R_{sh} extracted from TLM.

Since there can be considerable variation in the quality of emerging semiconducting materials, even on the same chip (e.g., variation in crystal quality in MoS_2), this can translate to a sizeable variation in R_{sh} from one device to another. Note, a perfect TLM is based on the assumption that R_{sh} is the same for all devices being tested, so any disruption to this assumption translates to inaccuracy in the extraction of R_c. Hence, it is highly recommended to fabricate several TLM device sets and plot the full distribution of resultant TLM data (multiple data points for each channel length). This provides evidence for how dependable the extraction is; a good example of this is in Ref. [9] and Fig. S5g below.

Another critical aspect of proper TLM data sets is the need for reporting the uncertainties of R_{sh} and R_c in standard error or confidence interval from a least-squares fit of the TLM curve; an example of this can be seen in Fig.2h and Ref. [10]. Lastly, if a record parameter is claimed based on TLM, four-probe measurements[7,11] should ideally be used as a complementary method to cross-check the results. Traditionally, four-probe measurements are used to characterize the resistivity of "bulk" doped films and a gate bias is not involved. However, to estimate the R_{sh} for emergent semiconducting materials, it is necessary to sweep the gate bias so that R_{sh} vs. gate voltage (carrier density, n_S) can be obtained. An example of the four-probe measurement is given in Fig. S3b. It is key to have probe 2 and 3 placed to the side of the channel so that the voltage probes (2 and 3) do not obstruct the current flow from probe 1 to 4. After obtaining R_{sh} vs. n_S, R_c vs. n_S can be derived by subtracting R_{sh} from R_{tot}.

A final caution regarding the use of TLM data is regarding the transfer length (L_T), which is the length of the contact over which the majority of carrier injection occurs between the metal and semiconductor. Traditionally, L_T was also extracted from TLM data as the intercept of the linear fit with the L_{ch} (x-axis). However, extracting L_T in this manner assumes that the sheet resistance of the semiconductor in the metal-contacted region is the same as for the semiconductor in the channel region. For emergent semiconducting materials, particularly low-dimensional materials like CNTs or 2D TMDs, this is not a valid assumption as transport through the materials happens predominantly (if not entirely) on the surface and is strongly dependent on the materials interfacing with the semiconductor. Because L_T has significant implications for the scalability of the contact length in emergent FETs, it must not be improperly extracted and reported from simple TLM data sets. This is commented on further in the next section (Note S4).

Note S4: Additional Parameters

In the main text, we covered the most representative parameters for reporting and benchmarking emergent FETs. Here we describe some additional parameters used in specific studies.

Normalization of I_D for 1D devices: For 1D or close to 1D devices, to compare I_D, it is sometimes necessary to convert the I_D per CNT/nanowire/nanosheet stack to I_D per µm. If the 1D channel materials are aligned CNTs or nanowires (Fig. S4a), the normalization of currents depends on the density of the 1D channel or the number of 1D channels in 1 µm. If the CNTs or nanowire are a dense network, treating the channel similar to a 2D material is more appropriate. For gate-all-around nanosheet devices (Fig. S4b), it is common to report I_D per nanosheet stack. If reporting the I_D per channel footprint, then the current per nanosheet stack should be divided by the nanosheet width (W_{NS}). A more detailed reporting of I_D per channel width would require the calculation total channel width of the nanosheets in the stack, which is close to $W_{NS} \times T_{NS} \times$ number of nanosheets in the stack. The normalized drain currents per channel width is I_D per stack divided by the total channel width of the stack. Ultimately, what matters is both an indication of what is achieved on a per nanomaterial/structure basis (e.g., per CNT or per nanosheet stack) as well as what is achieved on a per aerial footprint width basis (i.e., µA per W_{ch}).

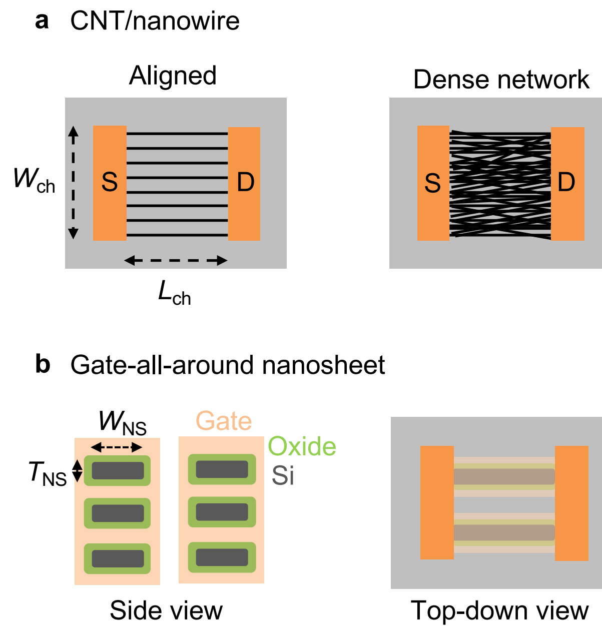

Fig. S4 | Normalization of currents for transistors based on 1D or close to 1D channel materials. **a**, top-down view of transistors based on CNTs or nanowires in the form of aligned channels and a dense network. **b**, side-view and top-down (aerial) view of gate-all-around nanosheet transistors.

Schottky barrier height: For Schottky contacts between metal and semiconductors, the Schottky barrier height determines the efficiency of carrier transport in the contacts. Hence, properly extracting the barrier height is key for comparing different contact engineering approaches. Examples of Schottky barrier extraction can be found in Ref. [3,12–14], with some variances in the equations and approaches used.

Transfer length (L_T): Because charge carriers tend to crowd near the contact edge when transported between the metal contacts and the channel material, only a certain portion of the contacts actively participate in the carrier transport process. The transfer length denotes the distance over which most of the current transfers in the contact. Traditionally, L_T can be estimated as $\sqrt{\frac{\rho_c}{\rho_{sh}}}$ from the transfer length method plot, where the ρ_c is the specific contact resistivity (unit: $\Omega\cdot cm^2$) and ρ_{sh} is the sheet resistance underneath the contact (unit: Ω/square) – this is discussed in some detail in Note S3 above. However, this estimation is not reliable for emergent transistors due to: 1) many of the emergent transistors use ultra-thin, low-dimensional nanomaterials, which can alter the current crowding behavior; 2) lots of research-grade emergent transistors have gated contacts, which complicates the estimation of the sheet resistance underneath the contact; and 3) the difference in the interface between the metal-semiconductor and gate insulator semiconductor leads to further differences in sheet resistance of the semiconductor in these regions. Hence, accurately determining L_T will depend on physically scaled contacts to observe the contact scaling behavior.

Interface trap density (D_{it}): This parameter is essential for studying and evaluating novel gate dielectrics. Different methods for determining D_{it} can be found in Ref. [12].

High-frequency response of the gate insulator capacitance: Although most of the parameters covered in the main text are low-frequency parameters, for devices to be eventually used in high-frequency and high-performance applications, it is necessary to properly evaluate the high-frequency response of the gate insulator capacitance and the current-voltage characteristics[15].

Note S5: Demonstration of device spread and parameter variations

As indicated in the main text, we recommend showing device spread and parameter variations to demonstrate the full picture of the reported devices. In Fig. S5, based on ten TLM structures similar to the one used in Fig. 2, we demonstrate the spread of device characteristics and parameter variations using a cumulative distribution function plot and boxplots.

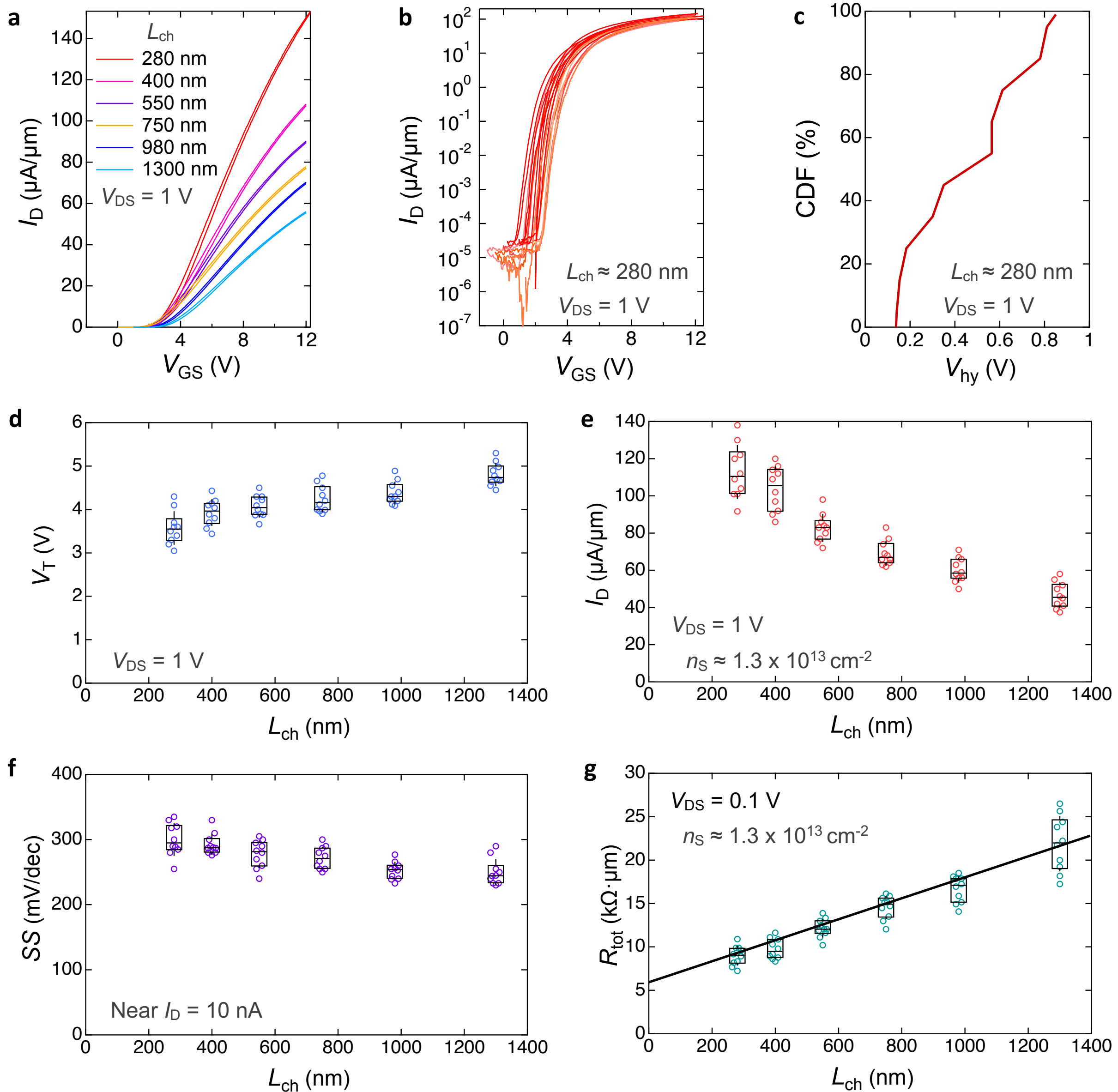

Fig. S5 | Demonstration of device spread and parameter variations based on ten TLM structures. **a**, Example transfer curves (I_D-V_{GS}) for the TLM structure in Fig. 2. **b**, Measured subthreshold curves (I_D-V_{GS}) of ten devices with L_{ch} of 280 nm of 280 nm. **c**, Cumulative distribution function (CDF) of the hysteresis voltage for the ten devices with L_{ch} of 280 nm. Boxplots of (**d**) V_T, (**e**) I_D at V_{DS} = 1 V and $n_S = 1.3\times10^{13}$ cm^{-2}, (**f**) the minimal *SS* extracted near I_D = 10 nA, and (**g**) ten TLM plots with the median R_c value of 3 kΩ·μm.

Note S6: Benchmarking devices with different channel thicknesses

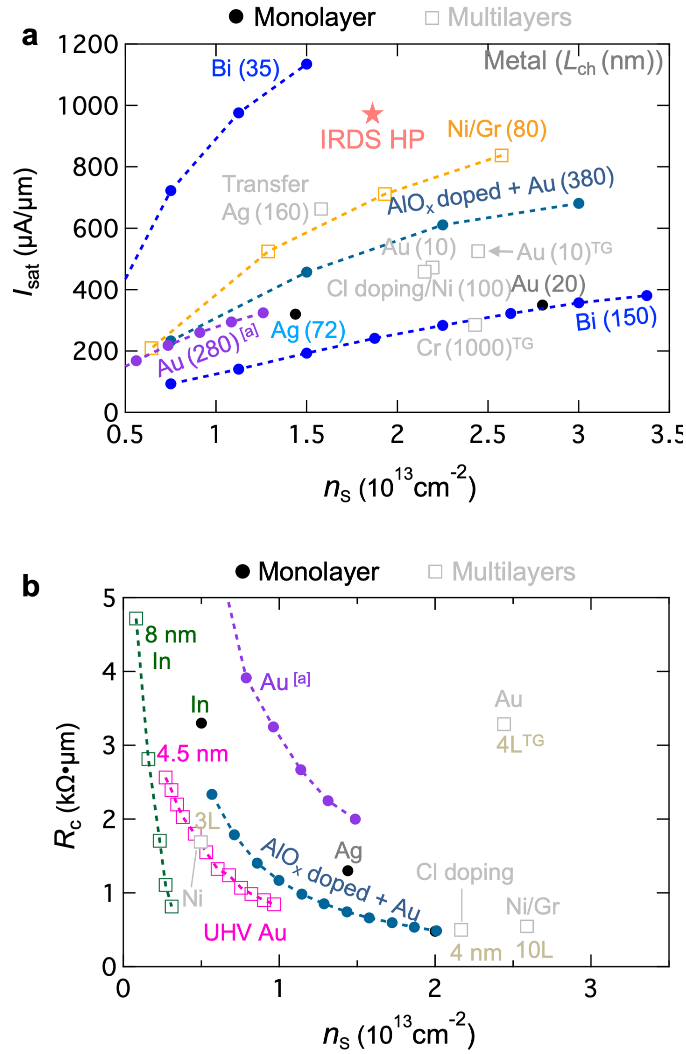

Fig. S6 | Example benchmarking device performance of MoS_2 FETs with different channel thicknesses. **a**, Benchmarking I_{sat} versus n_S, where the channel length in nm is labeled next to the metal contacts used in the devices. **b**, Benchmarking R_c versus n_S in a few representative reports, where the channel thickness is labeled for the multilayer channels. "a" stands for the example device in Fig. 2. A few studies are plotted as dotted lines to keep the plots from cluttering and also highlight the trends. Different colors are assigned to different reported devices. Most of the data are extracted from the following published reports: transferred Ag[16], AlO_x doped+Au[17], Ag[18], In[19], Ni [20], Cl doping[1], Ni/Gr[2], and Bi[3].

Representative reports with relatively large I_{sat} are listed in Table S1, with both monolayer and multilayer MoS_2 channels included.

Table S1| Representative reporting on studies of MoS_2 FETs with I_{sat}

Contacts	Ref.	t_{ch} (nm)	L_{ch} (nm)	n_S (10^{13} cm^{-2})	R_c (kΩ·μm)	V_{DS} (V)	I_{sat} (μA/μm)
Ag	[18]	1L	72	1.44	1.3	1.8	320
Au	[a]	1L	280	1.3	2	4	325
Au	[21]	1L	20	2.8	N/A	2	350
Bi	[3]	1L	150	3.4	0.12	2	380
Ni+Cl doping	[1]	4	100	2.16	0.5	1.6	460
Au	[21]	6	10	2.19	N/A	2	470
Sn	[22]	1L	35	1	0.84	1.5	615
Transferred Ag	[16]	4~20	160	1.58	N/A	3	660
AlO_x+Au	[17]	1L	380	2	0.48	5	700
Ni/Gr	[2]	10L	80	2.58	0.54	2	830
Ni	[23TG]	4.2	1000	2.43	N/A	3	290
Au	[24TG]	1L	10	~7	1.7	2	425
Cr	[25TG]	~4L	400	2.44	3.3	4	526

a: the example MoS_2 FET in Fig. 2a; TG = top gate; 1L = monolayer; 2L = bilayer, etc.
The Table lists I_{sat} in ascending order but not including the last three rows because they are top-gated. All other FETs were back-gated. μ_{FE} is not benchmarked as several of the studies listed have overestimated values. More studies that may not have I_{sat} reported can be accessed at Ref. [26].

References:

1. Yang, L. *et al.* High-Performance MoS_2 Field-Effect Transistors Enabled by Chloride Doping : Record Low Contact Resistance (0.5 k·µm) and Record High Drain Current (460 µA/µm). in *VLSI Technology* (2014).
2. Liu, Y. *et al.* Pushing the Performance Limit of Sub-100 nm Molybdenum Disulfide Transistors. *Nano Lett* **16**, 6337–6342 (2016).
3. Shen, P.-C. *et al.* Ultralow contact resistance between semimetal and monolayer semiconductors. *Nature* **593**, 211–217 (2021).
4. Ortiz-Conde, A. *et al.* A review of recent MOSFET threshold voltage extraction methods. *Microelectron. Reliab.* **42**, 583–596 (2002).
5. Ghibaudo, G. New method for the extraction of MOSFET parameters. *Electron. Lett.* **24**, 543–545 (1988).
6. Chang, H. Y., Zhu, W. & Akinwande, D. On the mobility and contact resistance evaluation for transistors based on MoS_2 or two-dimensional semiconducting atomic crystals. *Appl. Phys. Lett.* **104**, 113504 (2014).
7. Pang, C. *et al.* Mobility Extraction in 2D Transition Metal Dichalcogenide Devices—Avoiding Contact Resistance Implicated Overestimation. *Small* **17**, 2100940 (2021).
8. Streetman, B. G. & Banerjee, S. K. *Solid State Electronic Devices, 6th Edition*. (Pearson, 2006).
9. Kumar, A. *et al.* Sub-200 **Ω**·µm Alloyed Contacts to Synthetic Monolayer MoS_2. in *IEEE International Electron Devices Meeting (IEDM)* 154–157 (2021).
10. Smithe, K. K. H., English, C. D., Suryavanshi, S. V & Pop, E. Intrinsic electrical transport and performance projections of synthetic monolayer MoS_2 devices. *2D Mater.* **4**, (2016).
11. Guros, N. B. *et al.* Reproducible Performance Improvements to Monolayer MoS_2 Transistors through Exposed Material Forming Gas Annealing. *ACS Appl. Mater. Interfaces* **11**, 16683–16692 (2019).
12. Schroder, D. K. *Semiconductor Material and Device Characterization, 3rd Edition*. (Wiley-IEEE Press, 2015).
13. Das, S., Chen, H. Y., Penumatcha, A. V & Appenzeller, J. High performance multilayer MoS_2 transistors with scandium contacts. *Nano Lett* **13**, 100–105 (2013).
14. Cheng, Z. *et al.* Immunity to Contact Scaling in MoS_2 Transistors Using in Situ Edge Contacts. *Nano Lett.* **19**, 5077–5085 (2019).
15. Bethge, O. *et al.* Process temperature dependent high frequency capacitance-voltage response of ZrO2/GeO2/germanium capacitors. *Appl. Phys. Lett.* **96**, 052902 (2010).
16. Liu, Y. *et al.* Approaching the Schottky-Mott limit in van der Waals metal-semiconductor junctions. *Nature* (2018) doi:10.1038/s41586-018-0129-8.
17. McClellan, C. J., Yalon, E., Smithe, K. K. H., Suryavanshi, S. V. & Pop, E. High Current Density in Monolayer MoS_2 Doped by AlOx. *ACS Nano* **15**, 1587–1596 (2021).
18. Smithe, K. K. H., English, C. D., Suryavanshi, S. V. & Pop, E. High-Field Transport and Velocity Saturation in Synthetic Monolayer MoS_2. *Nano Lett.* **18**, 4516–4522 (2018).
19. Wang, Y. *et al.* Van der Waals contacts between three-dimensional metals and two-dimensional semiconductors. *Nature* **568**, 70–74 (2019).
20. Smets, Q. *et al.* Ultra-scaled MOCVD MoS_2 MOSFETs with 42nm contact pitch and 250µA/µm drain current. in *Technical Digest - International Electron Devices Meeting, IEDM* (2019). doi:10.1109/IEDM19573.2019.8993650.
21. Patel, K. A., Grady, R. W., Smithe, K. K. H., Pop, E. & Sordan, R. Ultra-scaled MoS_2 transistors and circuits fabricated without nanolithography. *2D Mater.* **7**, 015018 (2020).
22. Chou, A. S. *et al.* High On-State Current in Chemical Vapor Deposited Monolayer MoS_2 nFETs with Sn Ohmic Contacts. *IEEE Electron Device Lett.* **42**, 272–275 (2021).
23. Li, X. *et al.* Effect of Dielectric Interface on the Performance of MoS_2 Transistors. *ACS Appl Mater Interfaces* **9**, 44602–44608 (2017).
24. English, C. D., Smithe, K. K. H., Xu, R. L. & Pop, E. Approaching ballistic transport in monolayer

MoS_2 transistors with self-aligned 10 nm top gates. *Tech. Dig. - Int. Electron Devices Meet (IEDM)* 5.6.1-5.6.4 (2017) doi:10.1109/IEDM.2016.7838355.
25. Zou, X. *et al.* Interface engineering for high-performance top-gated MoS_2 field-effect transistors. *Adv. Mater.* **26**, 6255–6261 (2014).
26. McClellan, C. J. *et al.* 2D Device Trends. http://2d.stanford.edu.